Flux periodicity in a complex superconducting network

Xi Wang [1,2,*] Jincheng An,[3,*] Irina Volotsenko [1,2,4] Efrat Shimshoni [1] H. A. Fertig,[5,6]
Aviad Frydman [1,2,4] Ganpathy Murthy [3] and Beena Kalisky [1,2,†]
[1]*Department of Physics, Bar-Ilan University, Ramat Gan 5290002, Israel*
[2]*Institute of Nanotechnology and Advanced Materials, Bar-Ilan University, Ramat Gan 5290002, Israel*
[3]*Department of Physics and Astronomy, University of Kentucky, Lexington, Kentucky 40506, USA*
[4]*Jack and Pearl Resnick Institute, Bar-Ilan University, Ramat Gan 5290002, Israel*
[5]*Department of Physics, Indiana University, Bloomington, Indiana 47405, USA*
[6]*Quantum Science and Engineering Center, Indiana University, Bloomington, Indiana 47405, USA*

(Received 30 August 2024; revised 19 November 2024; accepted 3 December 2024; published 18 December 2024)

A basic feature of superconductors is flux quantization, which leads to periodicity of superconducting parameters with magnetic field. This periodicity is crucial for understanding basic concepts, such as elementary charge, symmetry of the order parameter, etc. In quantum circuit applications the periodicity is utilized for maximizing design performance. These applications rely on the fact that the periodicity is well defined for a given superconducting structure. We use scanning SQUID imaging and numerical simulations to show that, in realistic nanoscale devices, the periodicity depends on the temperature and the actual geometric details of the structure, specifically, the width of the wires that define the superconducting network. This should be taken into account in any experiment or application based on complex superconducting structures.

DOI: 10.1103/PhysRevB.110.214514

I. INTRODUCTION

One of the basic concepts in superconductivity is the quantization of flux, in units of $\Phi_0 = h/2e$, which manifests itself in diverse ways [1–5]. At temperatures below the superconducting transition temperature T_C, flux quantization leads to the appearance of superconducting vortices, forming vortex matter in type II superconductors. A well-known and early manifestation of this is the Little-Parks effect (LPE), i.e., the periodic oscillation of the critical temperature [3,6,7], critical current [8] (I_C), or the critical field [9–11] (H_C) as a function of magnetic flux in a superconducting loop. More generally, any nonuniform or periodic structure exhibits signatures of such periodicity. For example, in a periodic structure with a single type of hole in each unit cell, the periodicity of T_C as a function of flux per unit cell corresponds to the field required to accommodate one superconducting unit of flux ($\Phi_0 = \frac{h}{2e}$) through each unit cell: $B_{\text{period}} = \Phi_0/A_{\text{cell}}$, where A_{cell} is the geometric area of the unit cell. When one considers periodic networks with holes of different sizes, such as a kagomé network, the same idea works but can play out in somewhat more complicated ways, except now the periodicity is given by the change in the B field such that the smallest hole is being penetrated by one extra Φ_0. For example, in the kagomé lattice, with two triangular holes of geometric area A_t and one hexagonal hole of area $A_h = 6A_t$ per unit cell, a change of one Φ_0 through the triangular hole corresponds to a change of $8\Phi_0$ through the unit cell.

The exact determination of such periods is crucial both for applications and for basic physics [12,13]. An accurate measurement of the periodicity can be used to determine the basic charge unit in the system. Notably, the factor $2e$ in the definition of the flux quantum represents the charge of a Cooper pair, the elementary charge carrier in a conventional superconductor. In disordered superconductors and strongly correlated materials, the observation of unusual oscillation patterns may indicate more exotic states of matter; e.g., a topological phase [14], or coexisting charge order and superconductivity [15]. In applications, the periodicity is crucial for the design and operation of quantum computing elements like qubits and superconducting quantum interference devices (SQUIDs). Examples include the manipulation of topological states and the development of sensitive magnetometers [16,17].

The LPE is indeed universal because it describes physics near the critical point, where the important length scales in the problem, such as the London penetration depth λ_L, and the coherence length ξ, both diverge and, in particular, are much larger than the size of the unit cell a and the width w of the wires that make up the network.

The goal of our paper is to demonstrate, experimentally and theoretically, that this universality in the periodicity with respect to B is lost in kagomé networks at temperatures where $a,\ w > \lambda_L,\ \xi$, and that device geometry and structural details play key roles in setting the periodicity. This holds for any periodic network in which there are multiple holes with different areas in a unit cell.

In contrast to the LPE physics described above, at lower temperatures where these length scales turn finite, a more complex behavior arises, which depends on details of the

*These authors contributed equally to this work.
†Contact author: beena@biu.ac.il

network structure. The physics behind this lack of universality is conceptually simple. For $T \ll T_C$, assuming $w \gg \lambda_L, \xi$, the flux through each hole in the network must be strictly quantized to an integer multiple of Φ_0. The actual areas of the triangular holes $\tilde{A}_t$ and the hexagonal holes $\tilde{A}_h$ are no longer in the same ratio as the geometric areas in the $w \to 0$ limit. Furthermore, the presence of quantized fluxes in the holes sets up supercurrents, which generate magnetic moments. The supercurrents have kinetic energy, the quantized fluxes have magnetic field energy, and the magnetic moments have interaction energy. The system needs to find an arrangement of quantized fluxes, which minimizes these competing terms. We will show that true periodicity with B is lost, but an approximate periodicity emerges, which depends on the ratio of the actual areas of the holes $\frac{\tilde{A}_h}{\tilde{A}_t}$. We will also show that at generic values of total flux, there are a large number of competing states very close in energy, leading to freezing in local minima at low T.

The plan of this paper is as follows: In Sec. II, we provide a brief recapitulation of the LPE based on the treatment of Alexander [9]. This shows why at and near either T_C or H_C the problem can be considered linear, and also why the thickness of the wires does not matter for the LPE. In Sec. III, we present the experimental results obtained with a scanning SQUID on both square and kagomé networks. The square lattice follows the LPE periodicity, but the kagomé results show a clear deviation from the LPE periodicity of $8\Phi_0$ per unit cell for the kagomé lattice. In Sec. IV we present a simple model with only one free parameter incorporating the terms in the energy mentioned above, and show that it reproduces the experimental data quite well. In Sec. V we present some patterns of flux "fillings" for the two types of holes in the kagomé lattice, which appear at commensurate values of the flux per unit cell, and compare them to the results obtained from our model. Finally, in Sec. VI, we summarize our findings and explore some open questions.

II. PERIODICITY WITH RESPECT TO B NEAR T_C AND H_C

The conventional way of studying the periodicity of superconducting structures is by the LPE, where the resistance very close to the critical temperature is recorded as a function of the magnetic field [3,18]. Our brief introduction to the theory of the LPE will follow de Gennes [6,7] and Alexander [9]. We start with a thin wire ($w \ll \lambda_L, \xi$) implying that any variation of the superconducting order parameter Δ across the width of the wire is negligible, leaving it to vary along the length of the wire. This leads to the following Landau-Ginzburg free-energy functional for Δ:

$$F = \int d^3 r \mathcal{L}_{GL}(\Delta(\vec{r})),$$

$$\mathcal{L}_{GL} = -\alpha|\Delta|^2 + \frac{1}{2}\beta|\Delta|^4 + \frac{1}{2}\left|\hat{n}\cdot\left(i\nabla - \frac{2e}{\hbar}\vec{A}\right)\right|^2, \quad (1)$$

where $\alpha = \frac{T_C - T}{T_C} = \frac{1}{\xi^2}$, $\hat{n}$ is the unit vector along the wire, and $\vec{A}$ is the vector potential. Close to criticality, one makes the following well-justified approximations. (i) One neglects the nonlinear term in $\mathcal{L}_{GL}$ because Δ is very small near criticality. (ii) Now one considers a wire with its transverse dimensions much smaller than its length, implying that Δ depends only on the position along the wire. (iii) One now solves the equations of motion for Δ in the wire between sites i and j, provided the endpoint values Δ_i and Δ_j are specified. The solution is [6,7,9]

$$\Delta_{ij}(s) = \left(\Delta_i \frac{\sin((\ell_{ij} - s)/\xi)}{\sin\theta_{ij}} + \Delta_j e^{i\gamma_{ij}} \frac{\sin(s/\xi)}{\sin\theta_{ij}}\right) e^{-i\kappa_{ij}s},$$

$$\theta_{ij} = \ell_{ij}/\xi; \quad \kappa_{ij} = \frac{2e}{\hbar}\hat{n}\cdot\vec{A}; \quad \gamma_{ij} = \kappa_{ij}\ell_{ij}, \quad (2)$$

where ℓ_{ij} is the length of the wire joining sites i and j and s is a length variable measuring the position along the wire. The next step is to apply current conservation at each vertex, leading to the coupled linear equations [6,7,9]

$$-\Delta_i \sum_j \frac{\cot\theta_{ij}}{\xi} + \sum_j \Delta_j \frac{e^{i\gamma_{ij}}}{\xi \sin\theta_{ij}} = 0. \quad (3)$$

The critical temperature or applied magnetic field B is reached when this set of equations has no solutions with nonzero Δ. A key assumption in the solution of these equations is that since the superconductor is close to critical, screening supercurrents will be vanishingly small. Thus, the material is unable to screen the B field, implying that the B field is uniform, thus specifying A completely. This fact is what makes the solution so universal and independent of the width of the wires.

Based on this approach, we present the T_C versus field for the square and the kagomé lattices in Figs. 1 and 2. As can be seen, the square lattice T_C is periodic when the flux through each unit cell increases by Φ_0, while the kagomé lattice has a period of $8\Phi_0$.

III. LOW-TEMPERATURE RESULTS FOR THE SQUARE AND KAGOMÉ LATTICES

An alternative way of investigating the periodicity is to track the flux trapped in the structure by magnetic imaging. In recent decades, there have been several techniques employed to do this, such as scanning Hall microscopy [20], magnetic decoration [21], and scanning SQUID microscopy [22]. In this paper, we use the last of these to map the static magnetic landscape of superconducting Nb networks [see Fig. 1(a)] [23–25].

We begin with the simple case of a square lattice, for which we generated maps of the flux trapped in the grid cells after cooling it down through T_C in the presence of a fixed magnetic field. The evolution of flux patterns in this device is shown in Fig. 1(b). It is seen that each cell sequentially fills with a single Φ_0, resulting in two distinct value levels, corresponding to the presence of $n+1$ versus n flux quanta. The pattern evolves periodically, roughly displaying three distinct flux patterns: staircase and checkerboard at 1/3 and 1/2 fillings, respectively, and random near empty or full fillings.

As the magnetic field is increased, more cells are occupied, and when each cell accommodates one Φ_0, a new flux-filling cycle begins [Fig. 1(c)]. These observations are consistent with previous findings using a scanning Hall probe [20]. The periodicity extracted by locally imaging the flux patterns is identical to the periodicity of the LPE on the same structure, as

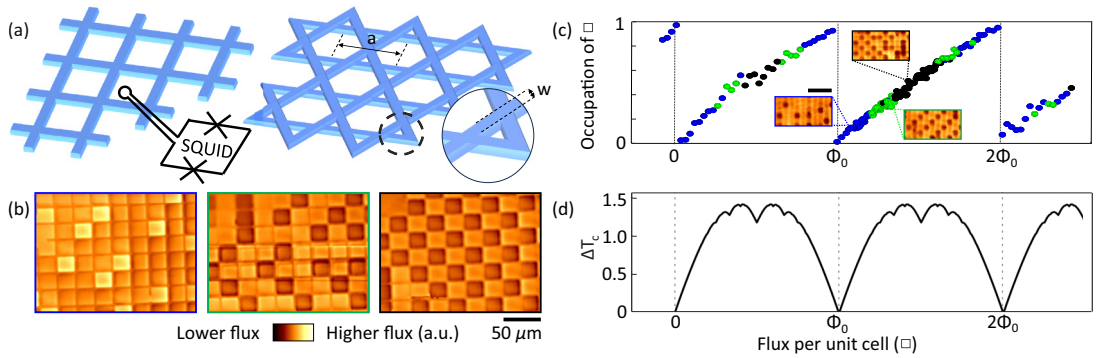

FIG. 1. Periodicity in a square cell network. (a) Illustrations of scanning SQUID measurement on a square and a kagomé lattice superconducting network. The lattice spacing is a and the width of the wires is w. (b) Flux trapped in the square network shows random configuration (filling factor 0.831), staircase (0.311), and checkerboard (0.484). In these images dark (light) color means lower (higher) amount of flux. For a quantitative explanation of the values and for raw data, see Figs. S1 and S2 within the Supplemental Material [19]. The flux difference between cells of different color amounts to one Φ_0, see Fig. S3 within the Supplemental Material [19]. (c) Occupation vs flux per unit cell. Each data point is calculated from a magnetic flux map showing the flux trapped in the network. Blue, random distribution; green, staircase; black, checkerboard. Insets are flux maps demonstrating the different configurations at filling factor 1.125, 1.413, and 1.532. Scale bar is 50 μm. (d) Calculated LP effect using the approach of Ref. [9].

shown in Fig. 1(d). This periodic behavior is well understood, as shown in previous experiments on a different structure with arrays of isolated rings [26,27].

The situation becomes much less trivial when dealing with patterns with more complicated unit cells, specifically ones that contain shapes of different sizes. For example, the flux configurations in triangular [28] and dice [29] lattices were mapped by magnetic decoration. However, with limited repetitions, these studies focused only on one or two commensurate filling factors. More complicated structures have

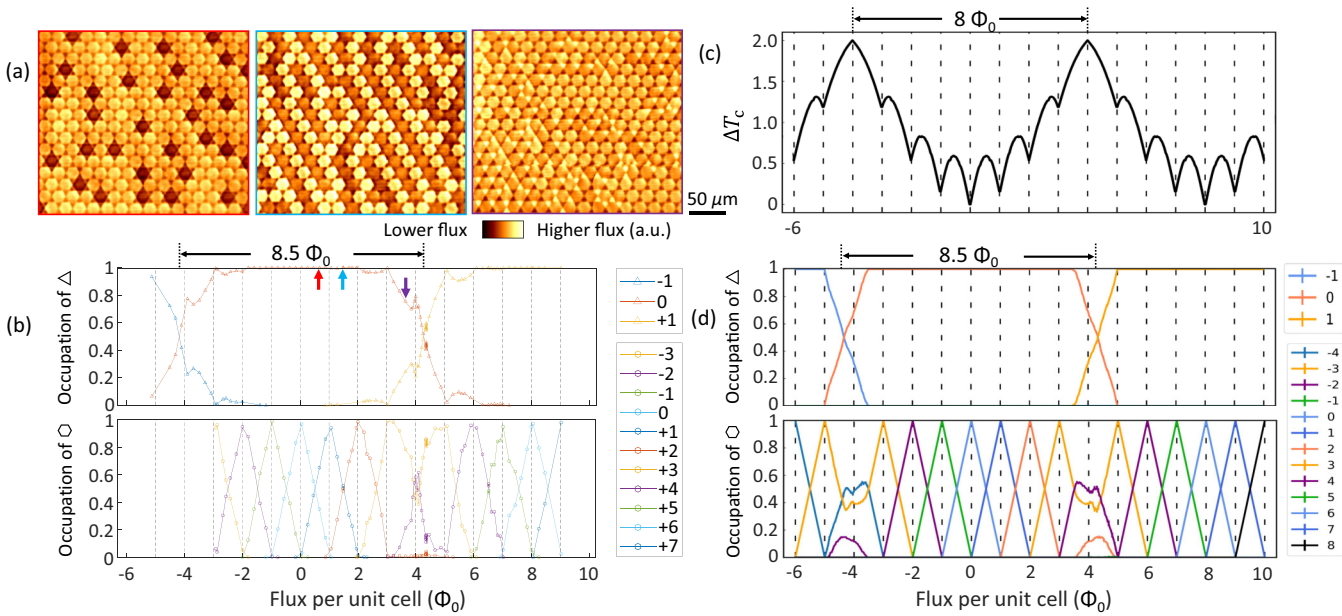

FIG. 2. Periodicity of the fillings of hexagons and triangles in a kagomé cell network as a function of flux. (a) Scanning SQUID images of representative flux configurations of the kagomé cell network. See Figs. S1 and S2 within the Supplemental Material [19] for raw data and the deconvolution process. The left two scans marked in red and blue show isolated and diagonal hexagon configurations, as the hexagons are slowly occupied while the triangles are empty. The right image (purple) shows the flux configuration when triangles are gradually filled. (b) Occupation vs flux per unit cell in the kagomé network for both triangle and hexagon cells. The arrows mark the magnetic field where the three images in panel a were taken. Each data point represents the occupation level extracted from the data, for both hexagons and triangles. Different symbol colors point to the level of flux in the pattern. The data captures three flux levels for the triangular and 11 for the hexagonal cells. For example, the blue arrow indicates that all triangles are at zero filling, with half of the hexagons filled by one Φ_0 while the other half is filled by two Φ_0. (c) Calculated LP effect using the approach of Ref. [9]. (d) Results from theoretical simulations, based on the actual ratio of areas of the holes in the device, $\tilde{A}_h/\tilde{A}_t = 7.84$. The ratio α/g was varied to fit the results of the simulation as closely as possible to the experiments, leading to $\alpha/g = 0.0824$. Note that in addition to the proper ratio of periods between the fillings of hexagonal holes and the triangular holes, the nonmonotonic filling of the hexagonal holes as the triangular holes become active is also reproduced.

been studied in the context of the LPE, including aperiodic structures like Penrose tilings [30,31], structures with tiles of irrational area ratios [32,33], and the kagomé lattice [34–36]. Here, we focus on a kagomé lattice, with a unit cell that is composed of a hexagon and two triangles that share a side, focusing on much lower temperatures than one does in LPE studies. In this paper, we studied a kagomé network that was fabricated by standard lithography techniques and had a hexagon side length of 8 μm and a non-negligible line width of 1 μm. The structure was composed of 50-nm-thick Nb sputtered on a Si substrate.

Following the flux-filling maps of the kagomé grid as a function of the field, we find that the hexagonal cells are "active" throughout most of the Φ_0 cycle, showing randomly filled hexagons, diagonal chains, and random holes [Fig. 2(a)]. The periodic hexagon filling cycle repeats itself over most of the field range, except for fields close to the half-filling of the triangular cells [Fig. 2(b)]. Interestingly, only in that narrow field range are the triangular cells "active". This behavior occurs because the energy cost of cell filling is inversely proportional to the area of the hole $\tilde{A}$. At small magnetic fields, the flux partially occupies the lower energy sites (the hexagons), forming patterns with increasing flux density that minimize the system energy. At high enough fields, it becomes energetically favorable to fill the triangles and their occupation takes over [Fig. 2(b)].

Surprisingly, the filling of the holes does *not* repeat when the applied magnetic flux through a unit cell is incremented by $8\Phi_0$, which would be the natural period for the LPE [3,34,35] since it represents an integral number of flux through each plaquette (a hexagon and two triangles). Indeed, the periodicity extracted from the SQUID measurements, $8.5\Phi_0$, and that expected from the LPE, $8\Phi_0$ [Fig. 2(c)], show a clear discrepancy. Very shortly, in the next section, we will propose and analyze a theoretical model, which explains this observation, and show that, depending on geometric details of the system, this difference in the periodicities can be much larger (see Sec. IV and Fig. 6 within).

Each point in Fig. 2(b) represents data extracted from a single cool-down at a specific field. Repeated cool-downs under the same field consistently yield the same results for the average occupations, although the images produced can vary significantly. For instance, we conducted eight cool-downs at a filling factor of 4.3, and the resulting occupations have a standard deviation of 0.014 for the triangle occupation and 0.019 for the hexagon occupation. Since this is smaller than the symbol size in the figures, we do not present error bars explicitly. Figure 3 displays data from four of these eight cool-downs at 4.3 fillings, illustrating the fact that while all show the same average occupations, the individual images (and thus the flux configurations) differ markedly from one another.

The occupation curve [Fig. 2(b)] exhibits interesting features, such as the skipped cycles of the triangles mentioned above. In the following, we list some of these features and use direct imaging of the flux configuration images to resolve their meaning.

Starting from zero filling and moving upward, just before the triangles begin to activate (filling 2–3), there is a small peak in the triangles' occupancy. The images reveal that the location of filled positive hexagonal cells forms clusters, and while preferring to sit together they repel positive filling of the triangles. The triangle filling is suddenly larger than zero (see Fig. 4). Around the filling factor 4, as the triangles' occupancy slowly increases, there is a sudden peak (or significant noise) observed in the occupation values.

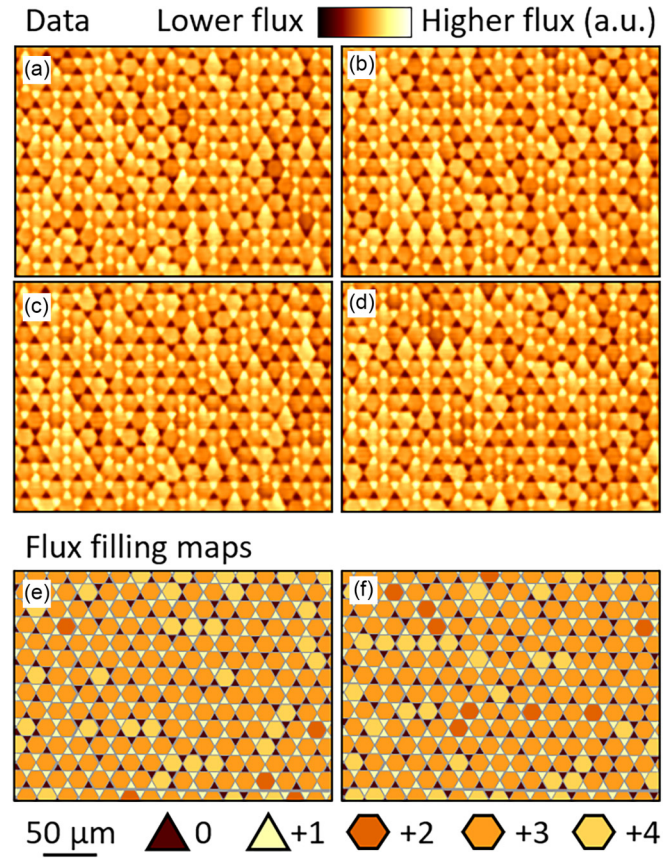

FIG. 3. Changes in the flux pattern of the kagomé network upon cycling the temperature above T_C and cooling back down. [(a)–(d)] Scanning SQUID images of flux configurations at fillings $4.3\Phi_0$ from different cool-downs. At this flux filling the average occupation of the triangles is one-half. The typical pattern at this magnetic field is complicated and changes upon temperature cycling. But the averaged occupations of triangles and hexagons are similar in each images. The deconvolution process, and the raw data are described in Figs. S1 and S2 within the Supplemental Material [19]. [(e)–(f)] Corresponding flux filling maps of panels (c) and (d). The flux levels represented by different colors are noted near the symbols.

Surprisingly, after the filling of the triangles is completed and the hexagonal filling returns to normal activity, there is a sudden increase in the triangles' occupancy around 5–6 filling. This activity appears stronger than the one near the peak observed at 2–3 filling. As explained in the next section, in our model this behavior is a consequence of the magnetic interactions between flux plaquettes.

IV. THEORETICAL MODEL AND RESULTS

The crucial difference between T close to T_C, as is the case in the LPE, and $T \ll T_C$, is the fact that in the LPE case the B field is uniform, and the problem is linear.

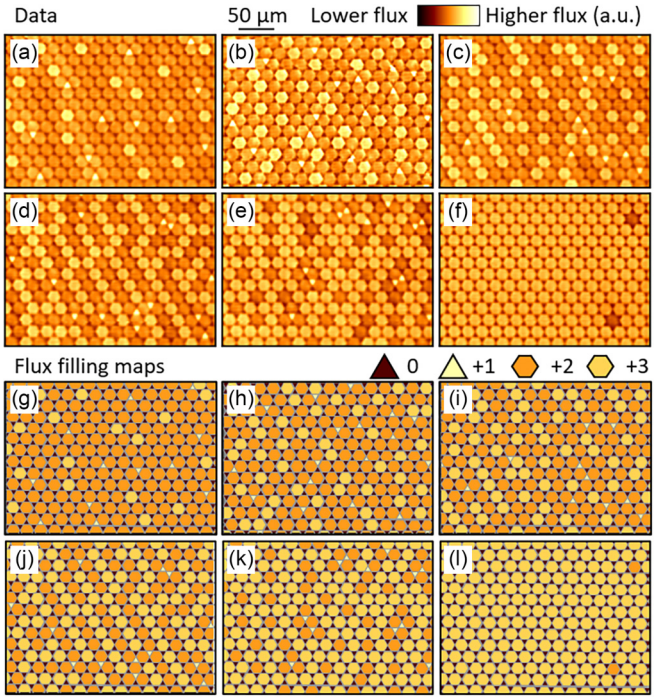

FIG. 4. Data showing an effective repulsion between the occupations of triangles and hexagons. [(a)–(f)] Scanning SQUID images of flux configurations of the kagomé cell network between a flux filling of 2 and 3. Flux per unit cell: 2.14, 2.41, 2.35, 2.54, 2.75, and 2.99. Before the triangles become active at filling 3, hexagons with occupation 3 (yellow) repel triangles with occupation 1 (yellow). At a flux filling of 3 only the hexagons are occupied. The deconvolution process, and the raw data are described in Figs. S1 and S2 within the Supplemental Material [19]. (e)–(l) Corresponding flux filling maps of panels (a)–(f).

As mentioned in the Introduction, for $T \ll T_C$ we have $\lambda_L, \xi \ll a, w$, which means that the B field vanishes inside the superconducting segments of wire. Recall that the width of the wires is about 1 μm, whereas niobiuim for $T \ll T_C$ has $\lambda_L \approx 0.04$ μm, $\xi \approx 0.05$ μm. The only caveat is that the thickness of the entire Niobium layer from which the network is made is $d \approx 0.05$ μm. Thus, the model that we present below should be thought of as an idealization of the real situation.

In the ideal situation with $d \gg \lambda_L$, the flux penetrating each hole has to be quantized and be an integer multiple of Φ_0. Here, we will proceed with this simpler model and discuss deviations for the realistic case $d \approx \lambda_L$ later.

The quantized fluxes in the holes are supported by circulating supercurrents in the network. In principle, the flux through a particular hole i depends on the currents throughout the network, but we make the simplifying assumption that the supercurrent circulating around a particular hole, and thus the magnetic moment m_i associated with that hole, depends only on ϕ_i. As we show within the Supplemental Material [19], the magnetic moments associated with the hole i is $m_i \propto \sqrt{\tilde{A}_i}\phi_i$, where $\tilde{A}_i$ is the area of the hole i. Importantly, $\tilde{A}_i$ is different from the geometric area A_i of a plaquette of a lattice with infinitely thin wires (see Fig. 5), because of the nonzero width w of each wire in the network. Once we make this assumption, it

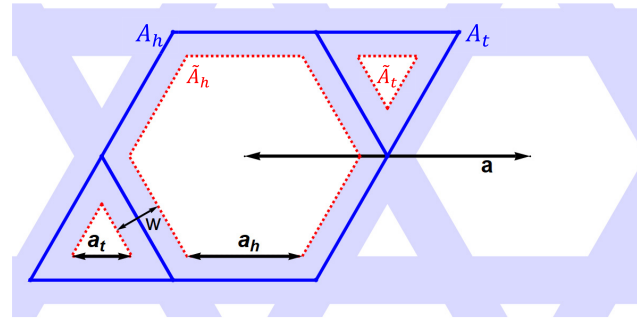

FIG. 5. Kagomé network with a lattice spacing a and wire width w. Note that area of a plaquette A_i (with $i = t$ for triangle, $i = h$ for hexagon, demarcated by solid blue lines) can be significantly different from the area of the corresponding hole in the network $\tilde{A}_i$ (demarcated by dashed red lines). For conditions close to criticality, such as the LPE, it is the plaquette areas A_i that matter, while at very low temperatures, when the fluxes through the holes are quantized, it is the areas of holes $\tilde{A}_i$ that matter.

is straightforward to write down a classical energy functional for the ϕ_i,

$$E(\{\Phi_i\}) = \alpha \sum_{i \neq j} \frac{\sqrt{\tilde{A}_i}\phi_i \sqrt{\tilde{A}_j}\phi_j}{|\vec{R}_i - \vec{R}_j|^3} + gd \sum_i \frac{\phi_i^2}{\tilde{A}_i} - \gamma \frac{\phi_{\text{ext}}}{A_{uc}} \sum_i \sqrt{\tilde{A}_i}\phi_i. \quad (4)$$

Here, the first term is the dipole-dipole interaction between m_i and m_j, with $\vec{R}_i$ denoting the position of the geometric center of the hole i. The second term, the self-energy of the flux ϕ_i, models the sum of the magnetic field energy of the flux going through the ith hole and the kinetic energy of the supercurrent producing ϕ_i, with d being the thickness of the wire in the z direction. The last term is the coupling of the magnetic moment to the external field. The coupling constants in the model are α, g, γ. By demanding that all the externally applied field goes through the holes (see the Supplemental Material [19]), one determines γ in terms of α, g. Assuming very low $T \ll T_c$, we use simulated annealing to find the minimum energy configurations, for which the overall energy scale is unimportant. Thus, there is only one free parameter in the model, the ratio α/g, which we fit to the experiment. As shown in Fig. 2(d), this simple model does a good job of reproducing the experimentally observed periodicity, including the nonmonotonic filling of the hexagonal holes when the triangular hole is being filled.

Let us delve deeper into the physics behind the discrepancy between LPE and flux configuration periodicities. The key quantity in determining the flux penetration into a superconductor is the penetration depth λ, which is replaced by $\lambda_{\text{eff}} = \lambda^2/d$ for thin films of thickness d. At T_c, $\lambda_{\text{eff}} \to \infty$ so that the magnetic field penetrates the entire film uniformly. This is the LPE regime. In a continuous film, for $T < T_c$, λ_{eff} is finite and a magnetic field penetrates in a nonuniform way, maximized at locations where the superconducting order parameter is zero (randomly located superconducting vortices).

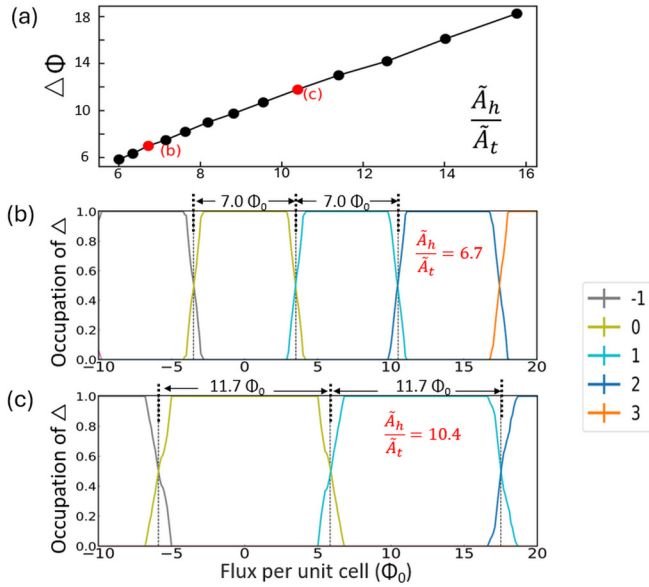

FIG. 6. Dependence of the approximate period of flux periodicity of the filling pattern on the kagomé lattice $\Delta\Phi$ on the width w of the wires. (a) $\Delta\Phi$ as a function of $\tilde{A}_h/\tilde{A}_t$. The period varies roughly linearly with the ratio of the actual areas, indicating its importance. (b) and (c) The filling of the triangular holes vs external flux at $\tilde{A}_h/\tilde{A}_t = 6.7$ and $\tilde{A}_h/\tilde{A}_t = 10.4$ for (b) and (c), respectively.

In a network, the location of these zeros is dictated by the geometry, as the film contains holes.

In this respect, the behavior is very different at T_C and well below T_C. In the LPE regime $T \leqslant T_C$, the penetration depth is infinite and hence $\lambda_{\text{eff}} \gg w$, whereas $T \ll T_C$ represents the opposite limit where $\lambda_{\text{eff}} \ll w$. Thus, in the low-temperature regime of our experiment, the flux does not penetrate the wire beyond a surface layer of thickness $\sim\lambda_{\text{eff}}$. This leads us to model the holes in the lattice through which the magnetic flux must be quantized, encircled by supercurrent loops generating magnetic dipole moments. The competition between the self-energy of the dipoles, their interactions with one another, and their coupling to the applied field determine the configurations of fluxes through the holes. Importantly, any periodicity of configurations is determined by the areas of the *holes* in the lattice, rather than the areas of the ideal *plaquettes*, so that the periodicity necessarily present in the LPE regime is modified. The model is able to broadly reproduce the behavior observed in the experiment [Fig. 2(d)] by tuning a single adjustable phenomenological parameter.

To demonstrate the role of the nonzero width w of the wire, we carried out simulations of our model with varying w/a, where a is the lattice spacing defined in Fig. 1(a). This leads to varying ratios $\tilde{A}_h/\tilde{A}_t$. As illustrated in Fig. 6, we find that as this ratio increases, the period of the triangle filling increases. This occurs because the self-energy of the triangular holes increases relative to that of the hexagonal holes as the ratio $\tilde{A}_h/\tilde{A}_t$ increases, and they become harder to fill. It is important to note that because of the nonlinear nature of the energy functional, and the fact that the fluxes ϕ_i are constrained to be integral, there is only an approximate periodicity. We can thus understand that the difference between the LPE and the low-temperature behavior of a superconducting wire array originates in the difference between minimizing the energetic phase stiffness cost at T_c, and the energetics of localizing its associated magnetic flux, which becomes dominant at low temperature.

The above discussion was based on the idealized assumption that the thickness of the superconductor $d \gg \lambda_L$. However, in the experiment, $d \approx \lambda_L$. Clearly, the B field will not be exactly zero within the superconductor, but will decay away from the holes. This can be taken into account by introducing an "effective" area for each hole $A_{t,\text{eff}}$, $A_{h,\text{eff}}$ whose values lie between the geometric areas of the corresponding plaquettes, and the actual areas of the holes. In fact, even in the ideal case, we should have done this, because our estimate for the field energy assumes that the field is uniform in the hole, while in reality it would be largest near the center of the hole and be smaller near the superconducting wires. There is enough freedom in the three parameters α, g, γ to accommodate these complicating effects. Thus, we conclude that the model continues to be valid, provided we interpret the parameters α, g, γ to incorporate correction factors for the difference between the actual areas of the holes and their effective area.

V. CONFIGURATIONS AT SPECIAL VALUES OF FLUX

In Sec. III we pointed out some interesting features of the data as the flux is varied. It turns out that the model can reproduce gross features of the data. For example, in the region of flux when the triangles are changing their filling, there is a nonmonotonic behavior of the hexagon filling. This is correctly reproduced by the model. In addition, while the triangles are inactive, only two flux fillings of the hexagon are ever observed. However, in the region where the triangles are active, a third occupation of the hexagons is observed in the data, and reproduced by the model.

The features of the data that the model fails to reproduce mainly concern sharp features such as the kinks in the triangle filling at flux per unit cell of ± 4. We believe this is the result of the small number of samples observed at this filling. The theoretical curve is the average of thousands of simulated annealing runs for each value of flux.

This brings up the issue of whether the experimental measurements correspond to samples in thermal equilibrium, or whether the configurations are frozen in local energy minima. Later in this section we will show scanning SQUID images at the same flux filling, but for different cool-downs, showing direct evidence that very different configurations are seen for different cool-downs (Fig. 3). We can also examine the same question in the model. There is a sharp dichotomy in the model results depending on whether the flux per unit cell is such that the triangles are active. For values of flux when the triangles are quiescent, although there are many distinct local minima accessed by simulated annealing, there is very little scatter in the values of the average occupations of the two types of holes. However, when the triangles are active, the scatter in the average occupations increases substantially. This trend is seen in Fig. 7, which shows the average occupations of the triangles and hexagons versus the energy of the local minimum at three different values of flux per unit cell.

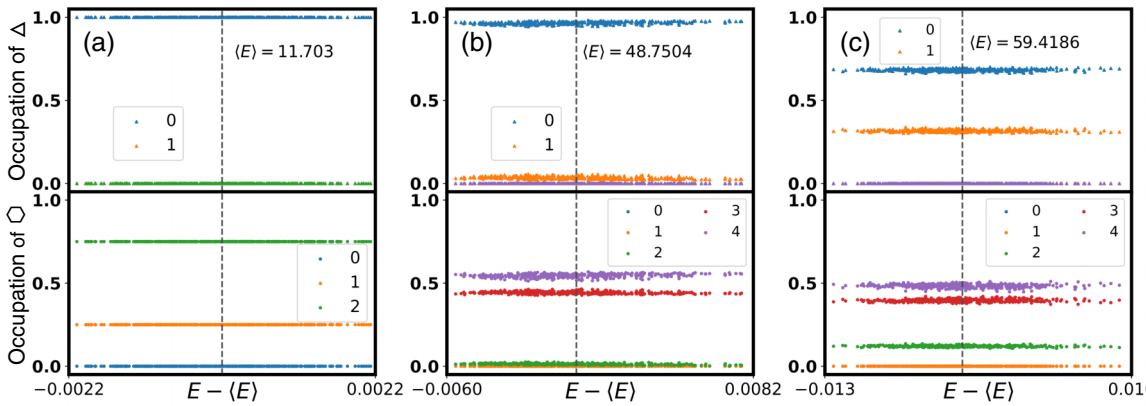

FIG. 7. Average occupations of the triangles and hexagons vs the energy of the local minimum at (a) $1.75\Phi_0$, (b) $3.6\Phi_0$, and (c) $4\Phi_0$ per unit cell. Simulated annealing is repeated 1000 times independently for each value of flux per unit cell. The black-dashed lines indicate the average of the local energy minima $\langle E \rangle$ in unit of g. (a) When the triangles are quiescent, there is very little scatter in the average occupations. This suggests that all local minima share the same average occupations. (b) and (c) When the triangles are active, scatter in average occupations increases significantly, suggesting that different local minima can have significantly different average occupations, leading to a lack of self-averaging.

These results suggest that in regions of flux where the triangles are actively filling, there is a lot more diversity in low-energy configurations accessible to the sample. Thus, one can expect more variations between samples, or even between different cool-downs of the same sample.

To examine this further, we look at the comparison between the experimental and theoretical configurations at the same value of flux. The parameters of the model have been fixed at the values that best fit the occupations versus flux data, as described in Sec. IV.

Figure 8 shows some experimental patterns as the filling changes around a filling of $4\Phi_0$, when the triangles are active. Panels (a)–(f) show the scanning SQUID images, with (a) corresponding to the lowest flux filling per unit cell of $3.68\Phi_0$ and (f) corresponding to the highest flux filling of $4.14\Phi_0$. The corresponding flux filling maps extracted from the data are shown in panels (g)–(l). Remarkably, in this region, we find domains that exhibit distinct structural patterns, each with a unique motif. For example, hexagons at filling $4\Phi_0$ are almost always surrounded by empty triangles, hexagons at filling $3\Phi_0$ are surrounded primarily by triangles with zero flux, while hexagons with filling $2\Phi_0$ are surrounded primarily by triangles at filling Φ_0. As the flux per unit cell increases, we see the domains with hexagons at filling $4\Phi_0$ surrounded by empty triangles growing. The size of these domains is $\approx$100 μm in the fields we examined.

In Fig. 9, we show some configurations obtained from simulated annealing based on our model, for the same sequence of fillings as in Fig. 8. As before, the theoretical results are much more regular than the experimental ones. However, we see the same motifs as in the experiment, namely, hexagons at $4\Phi_0$ surrounded by empty triangles, hexagons at $3\Phi_0$ surrounded by a mix of empty and singly filled triangles, and hexagons at $2\Phi_0$ surrounded by singly filled triangles. This gives us renewed confidence that our model is getting the short-distance physics approximately correct. Furthermore, the domains with $4\Phi_0$ hexagons surrounded by empty triangles grow as the flux filling increases, just as in the experiment. However, the domains in the simulation are far more regular. We attribute this to the disorder present in real samples, which is absent in the model. Each hole in a real sample has a slightly different area and shape, leading to small variations in the on-site energy and the magnetic moments associated with each hole. Another possibility is that the model is missing some residual short-range interactions, arising from our neglect of the

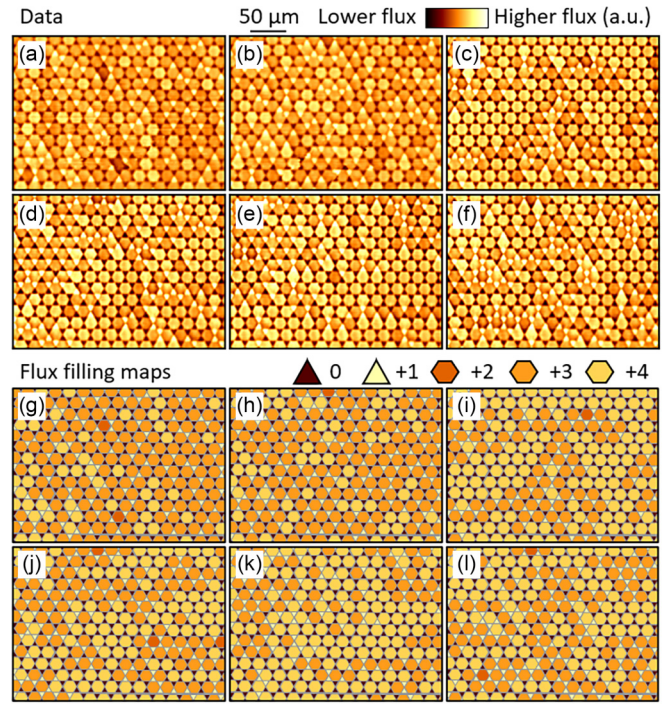

FIG. 8. Domain formation in the kagomé network when the triangles are active. [(a)–(f)] Scanning SQUID images of domain configurations near a flux filling of 4. Flux per unit cell: (a) 3.68, (b) 3.86, (c) 3.96, (d) 4.01, (e) 4.15, and (f) 4.14. The domain size gradually grows in these pictures. The deconvolution process, and the raw data are described in Figs. S1 and S2 within the SM [19]. (g)–(l) Flux filling maps extracted from the data of panels (a)–(f).

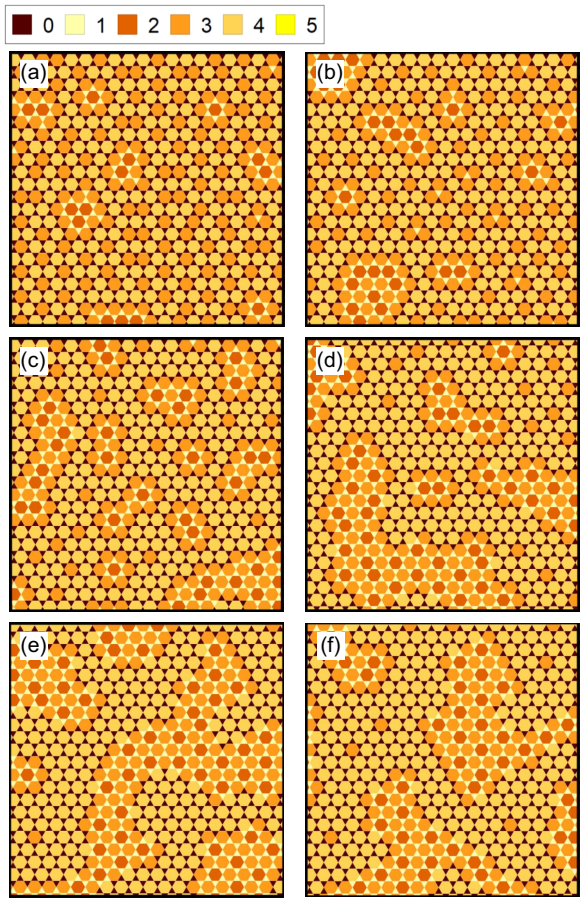

FIG. 9. Selected images of flux configurations of the kagomé cell network near fillings 4, based on simulated annealing of the model of Sec. IV. We use the same sequence of flux fillings as in Fig. 8. Flux filling per unit cell are (a) 3.68, (b) 3.86, (c) 3.96, (d) 4.01, (e) 4.15, and (f) 4.14.

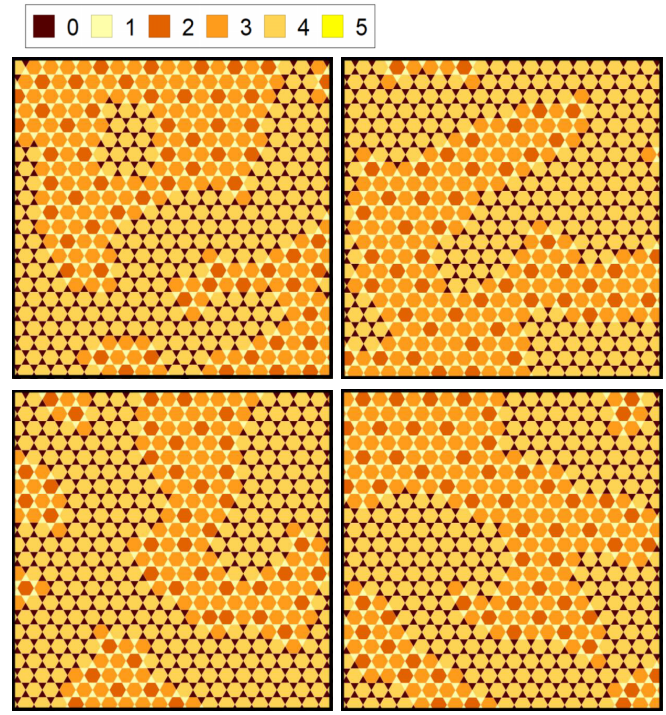

FIG. 10. Selected images of flux configurations of the kagomé cell network at fillings 4.3 based on simulated annealing of the theoretical model of Sec. IV. The same short-distance motifs show up as in the experiment, but the domains are larger and more regular than in the real data.

shapes of the holes, which could account for the difference in configurations. However, our model seems to contain the correct short-distance physics, which suggests that disorder is the likely reason for the differences between the experiment and our model results.

Figure 3 shows some experimental flux filling configurations for different cool-downs at a flux filling of 4.3 per unit cell. Panels (a)–(d) show the scanning SQUID images, while panels (e) and (f) show the flux filling in the triangles and hexagons extracted from panels (c) and (d) respectively, with the colors identified with different fillings. Now, we see hexagons at filling $2\Phi_0$ surrounded exclusively by triangles at unit filling, hexagons at filling $3\Phi_0$ and $4\Phi_0$ surrounded by a mix of empty and singly filled triangles. Hexagons with $3\Phi_0$ seem to dominate, with far fewer hexagons filled with $2\Phi_0$ or $4\Phi_0$.

In Fig. 10 we show four theoretical configurations from our model at the same filling of $4.3\Phi_0$ per unit cell. There are several differences between the experimental and theoretical results. The main difference is that the model configurations consist of large domains of almost periodic arrangements, whereas the experimental configurations are much more random. As discussed above, this is likely attributable to the inevitable disorder present in real samples. Furthermore, hexagons at filling $3\Phi_0$ seem to form a smaller fraction of hexagons in the simulation. In other words, the hexagon filling has a broader distribution in the simulation than in the experiments. This is actually evident in the comparison between Fig. 2(b) and Fig. 2(d). The experimental data shows only two nontrivial fillings of the hexagons, whereas the model shows three nontrivial fillings. The source of this discrepancy is unclear to us at present, though it must be rooted in the approximations we have made in constructing the model.

To summarize, by comparing the configurations seen in experiment to those seen in the simulation we conclude that the theoretical model has the correct short-distance physics, but fails to account for the sizes of domains seen in experiment. This discrepancy probably results from a combination of the disorder inherent in real samples, and the approximations made in the model.

VI. CONCLUSIONS

In conclusion, we have studied the low-temperature distribution of quantized magnetic flux in a superconducting wire array in a kagomé lattice with two different areas of plaquettes. We found two periodicities related to the same geometry. Near the critical temperature T_C the length scales related to superconductivity (the London penetration depth λ_L and the coherence length ξ) are much larger than the dimensions of the unit cell a or the thickness of the wires w making up the network. The resulting periodicity of T_C with respect to flux

is the universal Little-Parks periodicity, which is $8\Phi_0$ per unit cell for the kagomé lattice. However, for $T < T_C$, such that $a, w \gg \lambda_L, \xi$, the physics becomes nonuniversal. Now each hole in the lattice must have a flux that is strictly quantized in units of Φ_0. The distribution of these fluxes is governed by an energy functional containing the kinetic energy of the supercurrents around each hole, which we model as a "self-energy" of the flux occupying a hole, and the interaction energy of the magnetic moments thus formed. Making simplifying assumptions, we have constructed a simple model with only one free parameter, which reproduces many gross features of the data.

These findings have several important implications for both fundamental research and applied physics. The approximate periodicity we observe at low temperatures, governed by the ratio of the areas of the holes rather than the geometric areas of the plaquettes, suggests that device design and interpretation of experimental data in superconducting networks must carefully account for such geometric details. Moreover, our observation that self-averaging may be lost in certain flux regimes highlights the need for further investigation into the metastability and energy landscape of such systems, particularly in the context of quantum computing and other precision applications that rely on stable and predictable superconducting behavior.

Looking forward, several questions remain open. For example, how does the presence of disorder or variations in hole shapes and sizes further impact the flux configurations and periodicity in real-world devices? Additionally, what are the implications of these findings for other complex superconducting networks, such as those with different lattice symmetries or inhomogeneous materials? These questions point to a rich field of future research, where understanding the interplay between geometry, temperature, and magnetic flux could lead to new insights and technological advances.

ACKNOWLEDGMENTS

We thank S. Gur for the help in data analysis. X.W. and B.K. were supported by the European Research Council Grant No. ERC-2019- OG-866236, the Israeli Science Foundation Grant No. ISF-228/22, DIP 3970/1-1, and COST Action CA21144. A.F. and I.V. acknowledge support form the Israel Science Foundation (ISF) Grant No. 1499/21. E.S. acknowledges support of the Israel Science Foundation (ISF) Grant No. 993/19. J.A. is grateful to the University of Kentucky Center for Computational Sciences and Information Technology Services Research Computing for the use of the Morgan Compute Cluster. H.A.F. acknowledges the support of the NSF through Grant No. DMR1914451. E.S., H.A.F., and G.M. thank the Aspen Center for Physics (NSF Grant No. 1066293) for its hospitality, and financial support by the U.S.-Israel Binational Science Foundation through Award No. 2016130.

A.F. and I.V. prepared the samples. B.K. and X.W. performed SQUID measurements and data analysis. E.S., G.M., H.A.F., and J.A. developed the theory. All authors contributed to writing the manuscript.

[1] B. S. Deaver and W. M. Fairbank, Experimental evidence for quantized flux in superconducting cylinders, Phys. Rev. Lett. **7**, 43 (1961).

[2] R. Doll and M. Näbauer, Experimental proof of magnetic flux quantization in a superconducting ring, Phys. Rev. Lett. **7**, 51 (1961).

[3] W. A. Little and R. D. Parks, Observation of quantum periodicity in the transition temperature of a superconducting cylinder, Phys. Rev. Lett. **9**, 9 (1962).

[4] M. Tinkham, *Introduction to Superconductivity* (Krieger Publishing Company, New York, 1975).

[5] P. de Gennes, *Superconductivity of Metals and Alloys* (Addison-Wesley, Reading, MA, 1989).

[6] P. G. de Gennes, Diamagnetism of superconducting particles near a percolation threshold, C. R. Seances Acad. Sci. Ser. II **292**, 9 (1981).

[7] P. G. de Gennes, Critical field of a branched superconducting loop, C. R. Seances Acad. Sci. Ser. II **292**, 279 (1981).

[8] O. Buisson, M. Giroud, and B. Pannetier, Critical current of superconducting wire networks: Experimental study, Europhys. Lett. **12**, 727 (1990).

[9] S. Alexander, Superconductivity of networks. A percolation approach to the effects of disorder, Phys. Rev. B **27**, 1541 (1983).

[10] P. Gandit, J. Chaussy, B. Pannetier, and R. Rammal, Magnetic properties of a superconducting network, Phys. B: Condens. Matter **152**, 32 (1988).

[11] B. Pannetier and J. C. et R. Rammal, Experimental determination of the (H, T) phase diagram of a superconducting network, J. Physique Lett. **44**, 853 (1983).

[12] E. M. Spanton, M. Deng, S. Vaitiekėnas, P. Krogstrup, J. Nygård, C. M. Marcus, and K. A. Moler, Current–phase relations of few-mode InAs nanowire Josephson junctions, Nat. Phys. **13**, 1177 (2017).

[13] I. Sochnikov, A. J. Bestwick, J. R. Williams, T. M. Lippman, I. R. Fisher, D. Goldhaber-Gordon, J. R. Kirtley, and K. A. Moler, Direct measurement of current-phase relations in superconductor/topological insulator/superconductor junctions, Nano Lett. **13**, 3086 (2013).

[14] L. Fu and C. L. Kane, Josephson current and noise at a superconductor/quantum-spin-Hall-insulator/superconductor junction, Phys. Rev. B **79**, 161408(R) (2009).

[15] J. Ge, P. Wang, Y. Xing, Q. Yin, A. Wang, J. Shen, H. Lei, Z. Wang, and J. Wang, Charge-4*e* and charge-6*e* flux quantization and higher charge superconductivity in kagome superconductor ring devices, Phys. Rev. X **14**, 021025 (2024).

[16] D. Sabonis, O. Erlandsson, A. Kringhøj, B. van Heck, T. W. Larsen, I. Petkovic, P. Krogstrup, K. D. Petersson, and C. M. Marcus, Destructive Little-Parks effect in a full-shell nanowire-based transmon, Phys. Rev. Lett. **125**, 156804 (2020).

[17] T. Peng, A. W. Harrow, M. Ozols, and X. Wu, Simulating large quantum circuits on a small quantum computer, Phys. Rev. Lett. **125**, 150504 (2020).

[18] B. Pannetier, J. Chaussy, R. Rammal, and J. C. Villegier, Experimental fine tuning of frustration: Two-dimensional superconducting network in a magnetic field, Phys. Rev. Lett. **53**, 1845 (1984).

[19] See Supplemental Material at http://link.aps.org/supplemental/10.1103/PhysRevB.110.214514 for details of the assumptions underlying the effective model and the numerical simulations that underlie the results.

[20] H. D. Hallen, R. Seshadri, A. M. Chang, R. E. Miller, L. N. Pfeiffer, K. W. West, C. A. Murray, and H. F. Hess, Direct spatial imaging of vortices in a superconducting wire network, Phys. Rev. Lett. **71**, 3007 (1993).

[21] K. Runge and B. Pannetier, First decoration of superconducting networks, Europhys. Lett. **24**, 737 (1993).

[22] L. N. Vu, M. S. Wistrom, and D. J. Van Harlingen, Imaging of magnetic vortices in superconducting networks and clusters by scanning SQUID microscopy, Appl. Phys. Lett. **63**, 1693 (1993).

[23] M. E. Huber, N. C. Koshnick, H. Bluhm, L. J. Archuleta, T. Azua, P. G. Björnsson, B. W. Gardner, S. T. Halloran, E. A. Lucero, and K. A. Moler, Gradiometric micro-SQUID susceptometer for scanning measurements of mesoscopic samples, Rev. Sci. Instrum. **79**, 053704 (2008).

[24] E. Persky, I. Sochnikov, and B. Kalisky, Studying quantum materials with scanning SQUID microscopy, Annu. Rev. Condens. Matter Phys. **13**, 385 (2022).

[25] X. Wang, M. Laav, I. Volotsenko, A. Frydman, and B. Kalisky, Visualizing current in superconducting networks, Phys. Rev. Applied **17**, 024073 (2022).

[26] D. Davidović, S. Kumar, D. H. Reich, J. Siegel, S. B. Field, R. C. Tiberio, R. Hey, and K. Ploog, Correlations and disorder in arrays of magnetically coupled superconducting rings, Phys. Rev. Lett. **76**, 815 (1996).

[27] D. Davidović, S. Kumar, D. H. Reich, J. Siegel, S. B. Field, R. C. Tiberio, R. Hey, and K. Ploog, Magnetic correlations, geometrical frustration, and tunable disorder in arrays of superconducting rings, Phys. Rev. B **55**, 6518 (1997).

[28] B. Pannetier, A. Bezryadin, and A. Eichenberger, Imaging of vortices in 2D superconducting arrays: Magnetic decoration and other methods, Phys. B: Condens. Matter **222**, 253 (1996).

[29] E. Serret, P. Butaud, and B. Pannetier, Vortex correlations in a fully frustrated two-dimensional superconducting network, Europhys. Lett. **59**, 225 (2002).

[30] A. Behrooz, M. J. Burns, H. Deckman, D. Levine, B. Whitehead, and P. M. Chaikin, Flux quantization on quasicrystalline networks, Phys. Rev. Lett. **57**, 368 (1986).

[31] A. Behrooz, M. J. Burns, D. Levine, B. Whitehead, and P. M. Chaikin, Superconducting phase boundary of aperiodic networks in a magnetic field, Phys. Rev. B **35**, 8396 (1987).

[32] P. Santhanam, C. C. Chi, and W. W. Molzen, Flux quantization in periodic networks containing tiles with irrational ratio of areas, Phys. Rev. B **37**, 2360 (1988).

[33] P. Santhanam and C. C. Chi, Upper critical field of complex superconducting networks in the continuum limit, Phys. Rev. B **38**, 11843 (1988).

[34] Y.-L. Lin and F. Nori, Quantum interference on the kagomé lattice, Phys. Rev. B **50**, 15953 (1994).

[35] Y.-L. Lin and F. Nori, Quantum interference in superconducting wire networks and Josephson junction arrays: An analytical approach based on multiple-loop Aharonov-Bohm Feynman path integrals, Phys. Rev. B **65**, 214504 (2002).

[36] M. J. Higgins, Y. Xiao, S. Bhattacharya, P. M. Chaikin, S. Sethuraman, R. Bojko, and D. Spencer, Superconducting phase transitions in a kagomé wire network, Phys. Rev. B **61**, R894 (2000).